STUDY ON CRITICAL HEAT FLUX WITH NON-UNIFORM AXIAL HEAT FLUX DISTRIBUTIONS DURING LIFETIME IN REACTOR CORE

Dawei. Zhao, Wenxing. Liu, Yuanfeng. Zan, Wanyu. Xiong and Zumao. Yang
RETH, Nuclear Power Institute of China
Chengdu, Sichuan, 610041, China
zdw_npic@yahoo.com; flashfight@qq.com ; yfzan@163.com; wyxiong_114@163.com; zmyang_02@yahoo.com

ABSTRACT

Departure from nucleate boiling (DNB) type critical heat flux(CHF) is one of most important thermal criteria for nuclear reactor design. Concerning on the axial heat flux distributions at reactor core are non-uniform during the lifetime, it is of great significance to predict the critical heat flux under non-uniform heating conditions for reactor design and the performance promotion of reactor system. Some correction factors are proposed for the prediction of critical heat flux with non-uniform axial power shapes. Tong devised a correction factor model on the basis of the energy balance of bubble layer near the wall. On the basis of liquid sublayer dryout assumption by Lee and Mudawar, an improved mechanistic DNB-type critical heat flux model has been developed for non-uniform axial heat flux distribution. The non-uniform heat flux in axial is taken into account of upstream memory effect on potential boiling crisis point in this model. The boiling crisis is triggered when the liquid sublayer underneath vapor blanket is completely dried out by the local heat flux on the wall. The predictions of this improved mechanistic critical heat flux model and empirical correlations with correction factors are compared with the non-uniform heating CHF experimental results with three axial heat flux distributions. The comparison results show the present model has a reasonable prediction capability for DNB-type critical heat flux under non-uniform heating condition.

KEYWORDS
Critical heat flux, Non-uniform heating, Correction factor, Liquid sublayer dryout model

1. INTRODUCTION

The prediction of the critical heat flux (CHF) is of significant interest to the safety operations of nuclear reactor systems. There are many CHF prediction methods including empirical correlations, look-up tables and various mechanistic models for uniform heating condition. However, the axial heat flux distributions in reactor core are typical chopper-cosine heat flux profile with peak moving from the inlet to outlet during the whole lifetime. Therefore, it is of great significance to predict the q_{DNB} under non-uniform heating conditions for reactor design and the performance promotion of reactor system. Some correction factors are proposed for the prediction of CHF with non-uniform axial power shapes. The correction factor F_c is defined as the ratio of the CHF for the uniform flux case to the CHF for non-uniform flux case, $F_c=q_{cr,EU}/q_{cr,non}$. Tong devised a correction factor of non-uniform heat flux shape on the basis of the energy balance of bubble layer near the wall [1]. The F_c could be expressed by:

$$F_C = \frac{C_T \int_0^{z_{cr}} q_{loc}(z) e^{-C_T(z_{cr}-z)} dz}{q_{loc,cr}\left(1 - e^{-C_T z_{cr}}\right)} \quad (1)$$

where, z_{cr} is the boiling crisis point; $q_{loc}(z)$ is the local heat flux at z; $q_{loc,cr}$ is the local heat flux at boiling crisis point; the empirically determined expression for C_T is:

$$C_T = \frac{2.43(1-x_c)^{4.31}}{(G/1000)^{0.478}} \quad (2)$$

In present study**,** a mechanistic q_{DNB} model has been developed on the basis of liquid sublayer dryout mechanism, which is well accepted and widely used [2-6]. The non-uniform axial heat flux distribution is taken into account as upstream memory effect on boiling crisis in this model. The predictions of this improved mechanistic critical heat flux model and empirical correlations with correction factors are compared with the experimental results in the vertical tube with chopper-cosine axial heat flux distributions**.**

2. PROPOSED BOILING CRISIS MODEL

According to liquid sublayer dryout mechanism, vapor blankets are formed by small bubbles coalescence in boiling flow region, and a very thin liquid layer is underneath these vapor blankets near the heated wall.

The CHF is assumed to happen when the liquid layer is completely dried out and that spot on the heated wall is merely covered by vapor. Therefore, CHF can be expressed as:

$$q_{cr} = \rho_l \delta H_{fg} U_B / L_B \quad (3)$$

where δ, U_B, L_B are the thickness of liquid sublayer, the velocity and length of the vapor blanket, respectively.

The improved model is based on the following basic assumptions similar to those by Lee and Mudawar [4]:

(1) For subcooled or saturated flow boiling, bubbles in the flow channel detach the heated wall frequently after the net vapor generation (NVG) point. Then the detached bubbles coalescence into vapor blankets which overlay a very thin liquid sublayer in the near-wall region. The development of each vapor blanket is strongly influenced by neighboring blankets which tend to confine its circumferential growth. So it is reasonable to assume that the equivalent diameter of each blanket is approximately equal to the diameter of a bubble at the departure point from the wall.

(2) The velocity of the vapor blanket is the superposition of the local liquid velocity and the relative vapor blanket velocity, which is determined by a balance between buoyancy force and drag force exerted on the blanket in the flow direction.

(3) The blankets will stretch in the flow direction due to the evaporation of the liquid sublayer. And these blankets are interrupted by the Helmholtz instability effect at both interfaces on the two radial sides of the blankets, which will make the blankets intermittent. Thus, the vapor blanket length is assumed to be equal to the critical Helmholtz wavelength. And this assumption has been proved by Liu et al. [5].

(4) The non-uniform axial heat flux at upstream are integrated, make accumulative effect on local vapor blankets. Boiling crisis would be triggered when the liquid in the sublayer is completely evaporated by local heat flux, which induces the local heated wall directly covered by vapor blanket.

With the above assumptions, the proposed model can be depicted as follows:

2.1. Vapor Blanket Velocity U_B

The velocity of the vapor blanket is determined by a balance between the axial buoyancy force F_B and the drag force F_D [4]:

$$F_B = F_D \tag{4}$$

where

$$F_B = \frac{\pi}{4} D_B^2 L_B \left(\rho_l - \rho_g\right) g \tag{5}$$

$$F_D = \frac{1}{2} C_D \rho_l \left(U_B - U_{BL}\right)^2 \frac{\pi D_B^2}{4} \tag{6}$$

where D_B and L_B are the equivalent diameter and the length of the vapor blanket, respectively; ρ_l and ρ_g are the liquid phase and vapor phase density, respectively; g is the gravitational acceleration; C_D is the drag coefficient; U_B is the absolute vapor blanket velocity relative to the heated wall and U_{BL} is the liquid velocity at the radial position corresponding to the centerline of the vapor blanket. (U_B - U_{BL}) represents the relative velocity of the vapor blanket relative to the liquid.

According to Lee and Mudawar and Liu et al. [4, 5], the motions of small bubbles are dominated by viscous forces under high pressure condition. The drag coefficient correlation recommended by Chan and Prince [7] are adopted in present model(Eq. (7)).

$$C_D = \frac{48\mu_l}{\rho_l D_B \left(U_B - U_{BL}\right)} \tag{7}$$

Combining Eqs.(4)-(7), the velocity of the vapor blanket could be expressed as follows:

$$U_B = U_{BL} + \left(\frac{2L_B \left(\rho_l - \rho_g\right) g}{\rho_l C_D} \right) \tag{8}$$

Karman velocity distribution equation is used here to determine the local velocity gradient:

$$\begin{cases} U_L^+ = y^+ & 0 \le y^+ < 5 \\ U_L^+ = 5.0 \ln y^+ - 3.05 & 5 \le y^+ < 30 \\ U_L^+ = 2.5 \ln y^+ + 5.5 & 30 \le y^+ \end{cases} \tag{9}$$

where, $U_L^+ = \frac{U_L}{U_\tau}$, $y^+ = y\frac{U_\tau}{\mu_l}\rho_l$, $U_\tau = \sqrt{\frac{\tau_w}{\rho_l}}$, and $\tau_w = \frac{fG^2}{2\rho_l}$.

It is found that the liquid velocity profile around the vapor blanket always belongs to the buffer region (namely, the second expression of Karman's equation). Thus the local liquid velocity equation used in the present model can be rewritten as:

$$U_L = \frac{f^{0.5}G}{\rho_l}\left[1.768\ln\left(y\frac{f^{0.5}G}{\mu_l}\right) - 2.916\right] \tag{10}$$

Hence, the liquid velocity at the distance $y = \delta + D_b/2$ from the wall is given by:

$$U_{BL} = \frac{f^{0.5}G}{\rho_l}\left\{1.768\ln\left[\frac{f^{0.5}G\left(\delta + D_B/2\right)}{\mu_l}\right] - 2.916\right\} \tag{11}$$

The friction factor f is Fanning friction factor and can be calculated by Blasius equation as:

$$f = \frac{0.046}{\mathrm{Re}^{0.2}} \tag{12}$$

2.2. Vapor Blanket Velocity U_b

With the previous assumptions, the equivalent diameter of the vapor blanket is calculated from Levy model [8] as:

$$D_B = 0.015\left(\frac{\sigma D}{\tau_w}\right)^{0.5} \tag{13}$$

The length of the vapor blanket is expressed as the Helmholtz critical wavelength,

$$L_B = \frac{2\pi\sigma\left(\rho_l + \rho_g\right)}{\rho_l\rho_g\left(U_B - U_{sb}\right)^2} \tag{14}$$

where U_{sb} is the liquid velocity in the sublayer. Since the liquid sublayer near the heated wall is very thin, its velocity is very small comparing to the vapor blanket velocity. Here we assumed that U_{sb} equals 0 and then Eq. (14) turns to:

$$L_B = \frac{2\pi\sigma\left(\rho_l + \rho_g\right)}{\rho_l\rho_g U_B^2} \tag{15}$$

2.3. The sublayer thickness δ

The thickness of the liquid sublayer is determined by a balance of the forces exerted on the vapor blanket in the radial direction. Lee and Mudawar brought forward two forces exerted on the vapor blanket in

opposite directions, the evaporation force and the lift force [4]. The evaporation force F_E, which is created by small bubbles generating from the liquid sublayer and transferring into the vapor blanket, will push the vapor blanket away from the heated wall. While this evaporation force is resisted by a lift force F_L, which is caused by the rotation of the vapor blanket due to the velocity difference between the two phases and the velocity gradient at the radial position of the vapor blanket in the boundary layer.

The force caused by evaporation to the vapor blanket is given by Lee and Mudawar [4]:

$$F_E = \rho_g U_{se}^2 D_B L_B \tag{16}$$

where U_{se} is the vapor velocity due to the liquid sublayer evaporation. It can be expressed as:

$$U_{se} = \frac{q_b}{\rho_g H_{fg}} \tag{17}$$

where q_b is the portion of the heat flux used for vaporization. Just before CHF, assuming that the heat transferred through the vapor blanket into the core region is negligible. The heat flux get into the liquid sublayer just beneath the vapor blanket is completely blocked into the sublayer and used for the liquid vaporization. Hence, q_b is equal to the total wall heat flux q here.

$$q_b = q \tag{18}$$

Combining Eqs. (16), (17) and (18), then Eq. (16) turns to:

$$F_E = D_B L_B q^2 \Big/ \left(\rho_g H_{fg}^2 \right) \tag{19}$$

Beyerlein et al. derived an expression for the lift force on a bubble in turbulent two-phase flow through a vertical tube [9] (see Eq. (20)). The lift force rised from the rotation of the vapor blanket is associated with the velocity difference between the two phases and the velocity profile in the boundary layer.

$$F_L = C_L \rho_l \left(U_B - U_{BL} \right) \frac{\partial U_L}{\partial y} \frac{\pi}{4} D_B^2 L_B \tag{20}$$

where U_L is the local liquid velocity, and C_L is a lift force coefficient which is relevant to turbulent fluctuations and local bubble concentration. Beyerlein *et al*. suggested that C_L is a function of average void fraction and Reynolds number, yet they have not given a specific expression [9]. Lee and Mudawar brought forward a correlation as follows [4]:

$$C_L = a_1 \, \mathrm{Re}^{a_2} \tag{21}$$

where a_1 and a_2 are two empirical constants. The two empirical constants ignored the effect of void fraction. This seems to be improper and the authors of the present work proposed new expressions for a_1 and a_2.

Using Eq. (10), the local velocity gradient at the position of the vapor blanket is approximated by:

$$\frac{\partial U_L}{\partial y} \approx \frac{U_L\big|_{y=\delta+D_B} - U_L\big|_{y=\delta}}{\left(\delta + D_B\right) - \delta} = 1.768 \frac{f^{0.5} G}{\rho_l D_B} \ln\left(\frac{\delta + D_B}{\delta}\right) \tag{22}$$

Combining Eqs. (8), (21) and (22), Eq. (20) turns to:

$$F_L = 1.964 C_L G D_B L_B^{1.5} \left(\frac{f}{C_D} \frac{\rho_l - \rho_g}{\rho_l} g\right)^{0.5} \ln\left(\frac{\delta + D_B}{\delta}\right) \tag{23}$$

The wall lubrication force F_{WL} and the Marangoni force F_M are also considered in present model. The wall lubrication force will push the bubbles in the near-wall region toward the centerline of the channel. The wall lubrication force is modeled by Antal et al. and expressed as [10]:

$$F_{WL} = L_B \frac{\pi D_B^2}{4} \frac{C_{WL} \rho_l \left(U_B - U_{BL}\right)^2}{D_B} \tag{24}$$

where C_{WL} is the wall lubrication coefficient and is given by:

$$C_{WL} = C_L \max\left(0, C_1 + C_2 \frac{D_B}{y_w}\right) \tag{25}$$

with coefficients C_1 and C_2 set to -0.01 and 0.05, respectively. This force is limited within $y_w < 5D_B$ for the present formulation.

The variation of surface tension with temperature is considered in terms of Marangoni force which was originally derived by Lahey and Drew as follows [11]:

$$F_M = \frac{\pi D_B^2}{2} \frac{\partial \sigma}{\partial T} \frac{\partial T}{\partial y} \tag{26}$$

Vandervort et al. pointed out that the Marangoni force will hold the bubbles near the heated wall [12]. It can become dominant under very high heat flux conditions. However, according to the calculation results of the present work, the Marangoni force is negligibly small in comparison with the other three forces exerted on the bubbles.

Based on the radial balance of the four forces exerted on the vapor blanket, we have:

$$F_E + F_{WL} - F_L = 0 \tag{27}$$

Substitute Eqs. (19), (23), (24) and (25) into Eq. (27), then the thickness of the liquid sublayer δ could be expressed as:

$$\delta = \frac{D_B}{\exp\left\{\dfrac{\dfrac{q^2}{\rho_g H_{fg}^2} + \dfrac{\pi}{4} C_{WL}\rho_l \left(U_B - U_{BL}\right)^2}{1.964 C_L G L_B^{0.5}\left[\dfrac{f}{C_D}\dfrac{\rho_l - \rho_g}{\rho_l} g\right]^{0.5}}\right\} - 1} \tag{28}$$

After δ is calculated, U_{BL} can be calculated from Eq. (11) and then we can get U_B and L_B from Eq. (8) and Eq. (15), respectively. A correctional δ can be recalculated from Eq. (28) using new U_B and L_B. The iteration process is required until these parameters converge. The CHF could be predicted by substituting δ, U_B and L_B into Eq. (3).

3. CALCULATION PROCEDURE FOR NON-UNIFORM HEATING CHF

Under non-uniform axial heat flux distribution condition, the local heat flux could be expressed as follow:

$$q_{loc}\left(z\right) = q_{ave} * F_p\left(z\right) \tag{29}$$

where, q_{ave} is the average heat flux on the whole test section, $F_p(z)$ is the power factor, a function of heat flux distribution in axial direction.

With non-uniform axial heat flux distribution, the boiling crisis could be triggered at the upstream of outlet. Under different inlet conditions, the boiling crisis point will migrate in axial direction between the heat flux peak and the outlet. Therefore, with given geometric and inlet conditions, potential boiling crisis points z_{pcr} ranges from the heat flux peak to outlet under non-uniform heating condition.

The CHF at each potential boiling crisis point $q_{loc,cr}(z_{pcr})$ will be calculated firstly. An initial average heat flux on the whole test section q_{ave0} is assumed. The proposed heat flux distribution on the whole test section could be calculated by Eq. (29). The integral of non-uniform heat flux distribution at the upstream of z_{pcr} is used to calculate incoming flow characters at potential boiling crisis point, δ, U_B, L_B and other parameters could be calculated with the local heat flux $q_{loc}(z_{pcr})$. A hypothesis CHF at potential boiling crisis point $q'_{loc,cr}(z_{pcr})$ will be determined by Eq. (1). As the difference between $q'_{loc,cr}(z_{pcr})$ and $q_{loc}(z_{pcr})$ larger than the error limit, q_{ave0} will be replace by a new average heat flux on the whole test section calculated by $q'_{loc,cr}(z_{pcr})$. The iteration procedure brings the hypothesis CHF $q'_{loc,cr}(z_{pcr})$ approach to $q_{loc,cr}(z_{pcr})$.

With the $q_{loc,cr}(z_{pcr})$, each potential boiling crisis point corresponds an average heat flux q_{ave}. Obviously, the boiling crisis will be firstly triggered at the potential boiling crisis point corresponding minimum average heat flux. The $q_{loc,cr}(z_{pcr})$ at this boiling crisis point is the CHF on the test section with non-uniform axial power shape.

4. VERIFICATION AND COMPARISONS WITH CORRECTION FACTOR METHOD

4.1. A proposed expression of lift force coefficient C_L

In present study, we use the uniform heating CHF experimental data to propose a new expression of the lift force coefficient, C_L, in the liquid sublayer dryout model.

The lift force coefficient, C_L, expression is shown in the following:

$$C_L = \left(40 + 700\left(\alpha - 0.4\right)^2\right)\mathrm{Re}^{-0.35-0.23\exp(1.8\alpha)} \tag{30}$$

where α is void fraction.

In Fig. 1, we compare CHF preditions, $Q_{cr,CAL}$, of liquid sublayer dryout CHF model and Bowring correlation[13] with uniform heating CHF experimental result, $Q_{cr,EXP}$, in two length test sections with outlet quality changing from -0.2 to 0.4.

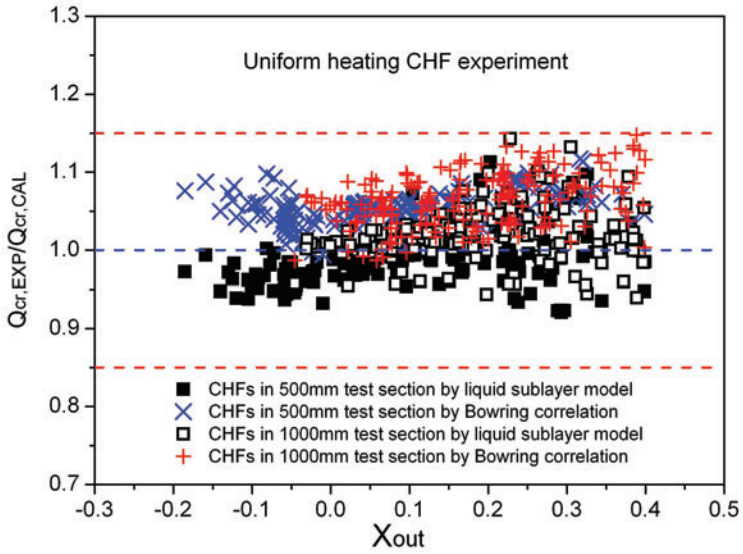

Figure 1. Comparisons between predictions and uniform heating experiment results.

The Bowring correlation is proposed for critical heat flux in single tube under uniform heating conditon:

$$Q_{cr} = \frac{A' + 250D_i G\Delta h_{in}}{C' + L} \tag{32}$$

where,

$$A' = \frac{2.317\left(250h_{fg}D_i G\right)F_1}{1.0 + 0.0143F_2 D_i^{0.5} G} \tag{33}$$

$$C' = \frac{0.077F_3 D_i G}{1.0 + 0.3473F_4\left(G/1356\right)^n} \tag{34}$$

$$n = 2.0 - 0.5\left(P/6.895\right) \tag{35}$$

$$F_1 = \begin{cases} \left(\left(P/6.895 \right)^{18.942} e^{20.8\left(1-\left(P/6.895\right)\right)} + 0.917 \right) \Big/ 1.917 & P < 6.895 MPa \\ \left(P/6.895 \right)^{-0.368} e^{0.648\left(1-\left(P/6.895\right)\right)} & P > 6.895 MPa \end{cases} \quad (36)$$

$$F_1/F_2 = \begin{cases} \left(\left(P/6.895 \right)^{1.316} e^{2.444\left(1-\left(P/6.895\right)\right)} + 0.309 \right) \Big/ 1.309 & P < 6.895 MPa \\ \left(P/6.895 \right)^{-0.448} e^{0.245\left(1-\left(P/6.895\right)\right)} & P > 6.895 MPa \end{cases} \quad (37)$$

$$F_3 = \begin{cases} \left(\left(P/6.895 \right)^{17.023} e^{16.658\left(1-\left(P/6.895\right)\right)} + 0.667 \right) \Big/ 1.667 & P < 6.895 MPa \\ \left(P/6.895 \right)^{0.219} & P > 6.895 MPa \end{cases} \quad (38)$$

$$F_4/F_3 = \left(P/6.895 \right)^{1.649} \quad (39)$$

As shown in Fig.1, $Q_{cr,CAL}$ by liquid sublayer dryout CHF model show a reasonable agreement with uniform heating $Q_{cr,EXP}$ using new proposed C_L expression. The error band of $Q_{cr,CAL}$ by Bowring correlation are range from -3% to 15%. Most $Q_{cr,CAL}$ by Bowring correlation are smaller than the CHF experimental results, $Q_{cr,EXP}$.

4.2. Verfication using non-uniform heating CHF experiments

The non-uniform heating CHF experiments are conducted with inlet-peak, center-peak and outlet-peak heat flux profiles, which correspond to the axial heat flux distributions at the beginning, mid-term and ending lifetime in reactor core. The narrow rectangular cross-section is the same in uniform heating and non-uniform heating CHF experiments with a gap in 2mm. The wall outside thickness for each heat flux profile test section is in inverse proportion with the axial heat flux distribution. DC power supply is employed to heat the tube ohmically. From the outlet, there are at least 20 wall temperature sections along the axial direction of heated section. The distance between wall temperature sections are 15mm. Each temperature section has 6 type-K thermocouples spot-welded directly on the tube surface to measure the wall temperatures and detect the trigger and positions of CHF. The predictions by present model and correction factor method are compared with those non-uniform heating CHF experimental data. For correction factor method, non-uniform axial heat flux distribution factor F_c devised by Tong (Eq.1 and Eq.2) is adopted to correct the uniform heating CHF calculated by Bowring correlation.

As shown in Fig.2, the non-uniform heat flux profile is chopper-cosine shape with peak near the inlet of test section. In the inlet-peak CHF experiments, boiling crisis is triggered at the outlet far from the heat flux peak with quality ranges from 0.1 to 0.4. The boiling crisis positions predicted by liquid sublayer dryout model and correction factor method are also at the outlet. The CHF predictions both show a reasonable agreement with experimental results.

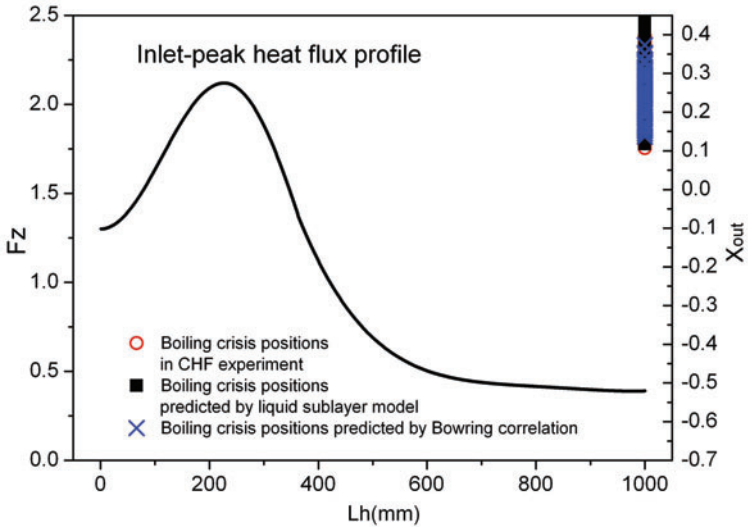

(a) Axial heat flux profile and boiling crisis points

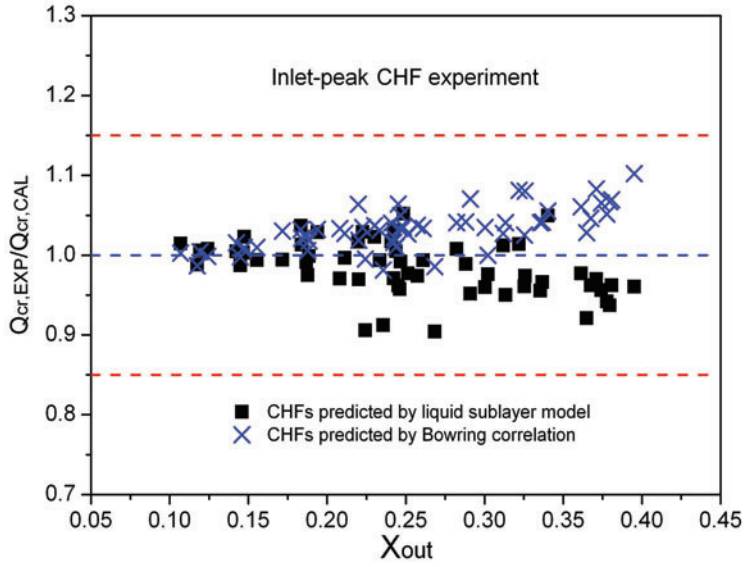

(b) CHFs under inlet-peak heat flux profile conditions

Figure 2. Comparisons between predictions and inlet-peak CHF experiment results.

In Fig.3, the non-uniform heat flux profile is chopper-cosine shape with peak almost at the middle of test section. In the center-peak CHF experiments, boiling crisis is still triggered at the outlet with quality ranges from 0.05 to 0.4. The boiling crisis positions predicted by liquid sublayer dryout model are also at the outlet. And the CHF and averaged heat flux predictions are agreed well with experimental results. However, the boiling crisis positions are moving to the outlet upstream under low quality conditions using correction factor method. Therefore, the relative powers at the predicted boiling crisis position are bigger than at the outlet. Those CHFs at upstream of outlet show notable deviations in correction factor method, although most averaged heat flux predictions are still in $\pm$15% error band.

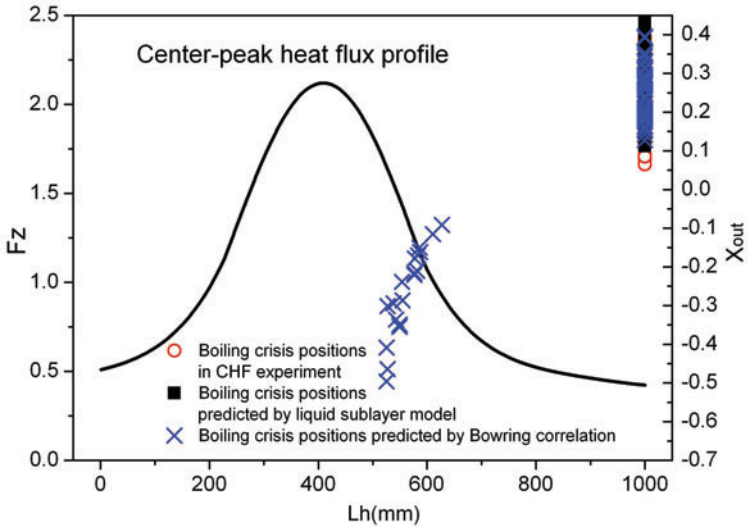

(a) Axial heat flux profile and boiling crisis points

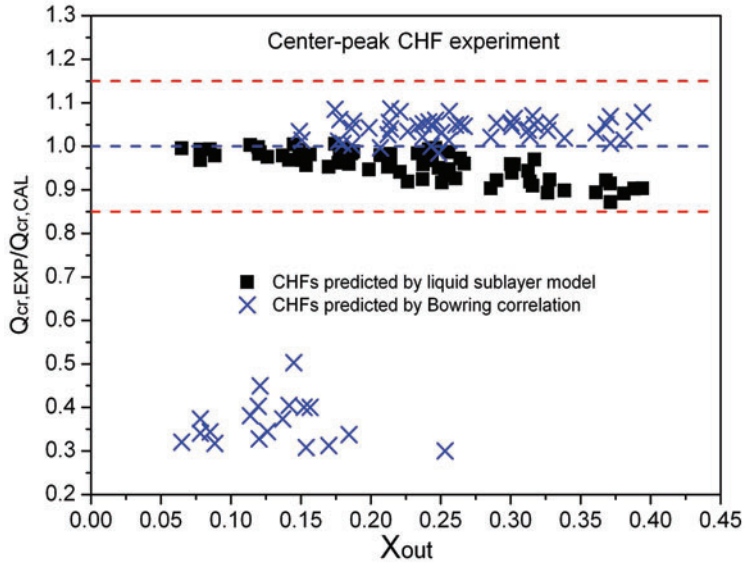

(b) CHFs under center-peak heat flux profile conditions

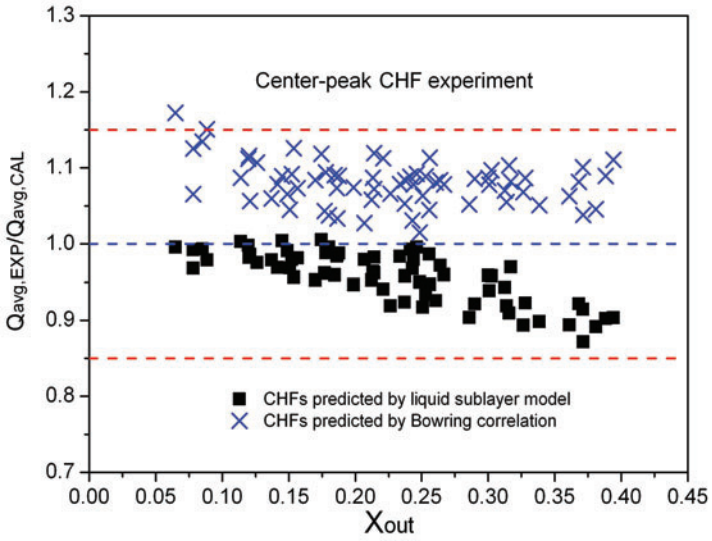

(c) Averaged axial heat fluxes at boiling crisis

Figure 3. Comparisons between predictions and center-peak CHF experiment results.

In Fig.4, the non-uniform heat flux profile is chopper-cosine shape with peak near the outlet of test section. In the outlet-peak CHF experiments, even through the quality ranges to -0.1, boiling crisis is still triggered at the outlet. However, several boiling crisis positions predicted by liquid sublayer dryout model and correction factor method are moving to heat flux peak at the upstream of outlet. For correction factor method, the CHF and averaged heat flux predictions could fall in a reason error band when the predicted boiling crisis positions are at outlet. As the boiling crisis positions moving to heat flux peak, the boiling crisis is expected to be triggered by the higher local heat flux at outlet upstream while the averaged heat flux are still lower than the experimental results. For liquid sublayer dryout model, the boiling crisis position departs quit short distance from the outlet. The CHF and averaged heat flux predictions are agreed well with experimental results when the predicted boiling crisis positions are at outlet. As the boiling crisis positions moving to heat flux peak, the boiling crisis is also triggered by the higher local heat flux at outlet upstream. However, the averaged heat fluxes are still keep a reasonable agreement with the experimental results.

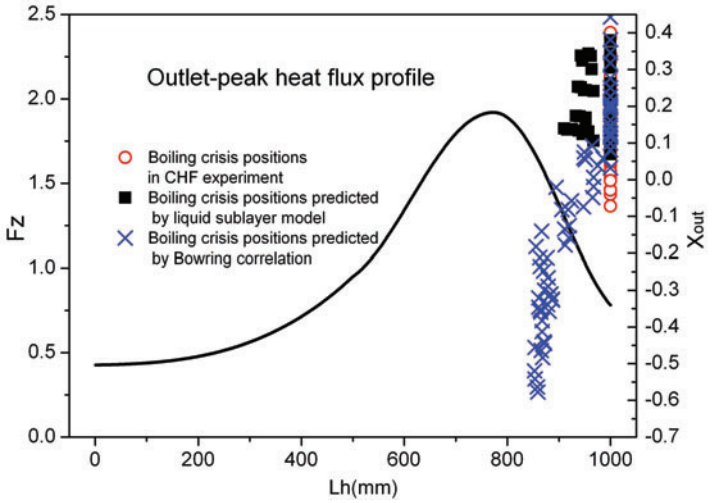

(a) Axial heat flux profile and boiling crisis points

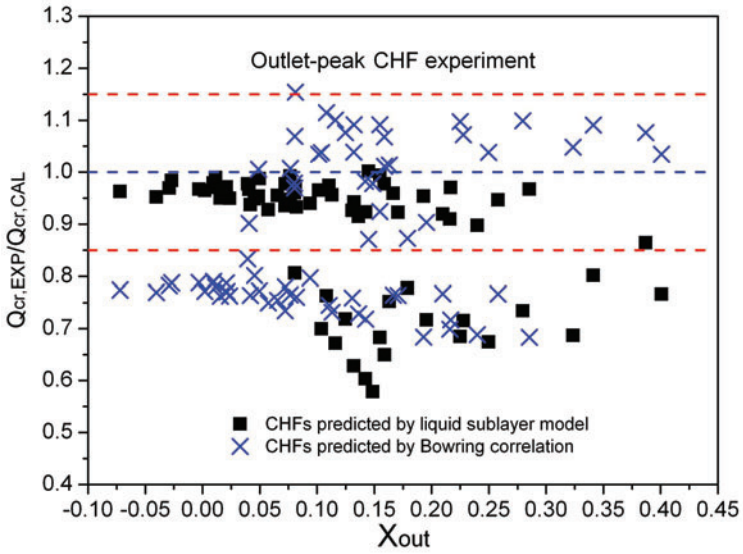

(b) CHFs under outlet-peak heat flux profile conditions

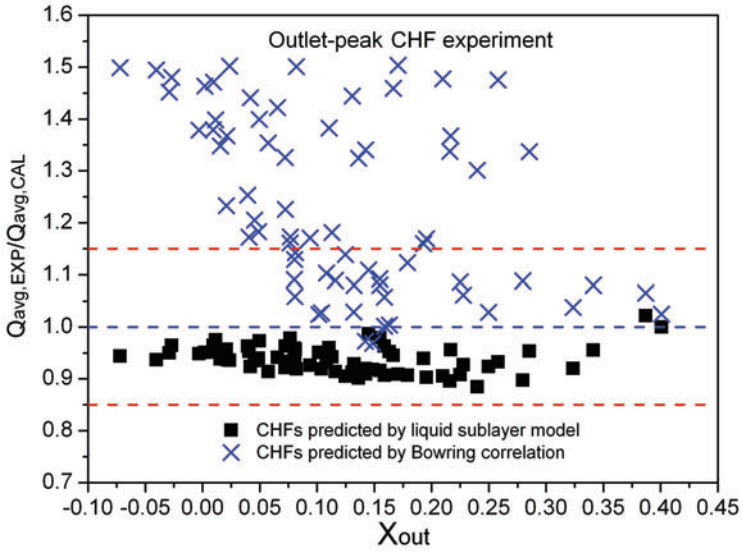

(c) Averaged axial heat fluxes at boiling crisis

Figure 4. Comparisons between predictions and outlet-peak CHF experiment results.

5. CONCLUSIONS

In present three non-uniform heating CHF experiments, the axial heat flux is changing continuously. There are no step changes or interruptions in the axial heat flux profile. Therefore, we assume the trigger mechanics of boiling crisis with slowly changing axial heat flux couldn't be significant different with uniform heating condition. The non-uniform heating CHF could be predicted based on uniform heating liquid sublayer dryout mechanism. In present study, the non-uniform axial heat flux distribution at the upstream is considered to make cumulative effect on the incoming flow characters at boiling crisis point. The local heat flux at boiling crisis point is taken as the triggering threshold basis on liquid sublayer dryout mechanism. The comparisons between the predictions by the liquid sublayer model and experiment results of inlet-peak and center-peak CHF experiments show a reasonable accuracy with CHF

deviation ranges from -14% to 5%. However, for outlet-peak CHF experiment, the CHF deviations are notable when the predictions of boiling crisis points depart from experimental results. As heat flux peak is near the outlet, the heat flux distribution is changing notable at the boiling crisis point. The influences of non-uniform heating flux profile on boiling crisis may not be neglected. The further research should focus on non-uniform heating effects on boiling crisis trigger mechanics.

ACKNOWLEDGMENTS

This work was supported by the National Natural Science Foundation of China through grants No. 51406189.

REFERENCES

1. L.S. Tong, "Prediction of Departure from Nucleate Boiling for an Axially Non-Uniform Heat Flux Distribution", *Journal of Nuclear Energy*. **21**, pp. 241-248 (1967).
2. G.P. Celata, M. Cumo, A. Mariani, M. Simoncini, G. Zummo, "Rationalization of Existing Mechanistic Models for the Prediction of Water Subcooled Flow Boiling Critical Heat-Flux", *International Journal of Heat and Mass Transfer*. **37**, pp. 347-360 (1994).
3. Y. Katto, "A prediction model of Subcooled Water-Flow Boiling CHF for Pressure in the Range 0.1-20-MPa", *International Journal of Heat and Mass Transfer*. **35**, pp. 1115-1123 (1992).
4. C.H. Lee, I. Mudawar, "A Mechanistic Critical Heat Flux Model for subcooled flow boiling based on Local Bulk Flow Conditions", *International Journal of Multiphase Flow*. **14**, pp. 711-728 (1988).
5. W. Liu, H. Nariai, F. Inasaka, "Prediction of Critical Heat Flux for Subcooled Flow Boiling", *International Journal of Heat and Mass Transfer*. **43**, pp. 3371-3390 (2000).
6. L.A. Payan-Rodriguez, A. Gallegos-Munoz, G.L. Porras-Loaiza, M. Picon-Nunez, "Critical Heat flux Prediction for Water Boiling in Vertical Tubes of a Steam Generator", *International Journal of Thermal Science*. **44**, pp. 179-188 (2005).
7. B.K.C. Chan, R.G. H. Prince, "Distillation Studies - Viscous Drag on a Gas Bubble Rising in a Liquid", *Aiche Journal*. **11**, pp. 176-192 (1965).
8. S. Levy, "Forced Convection Subcooled Boiling - Prediction of Vapor Volumetric Fraction", *International Journal of Heat and Mass Transfer*. **10**, pp. 951-965 (1967).
9. S.W. Beyerlein, R.K. Cossmann, H.J. Richter, "Prediction of Bubble Concentration Profiles in Vertical Turbulent 2-Phase Flow", *International Journal of Multiphase Flow*. **11**, pp. 629-641 (1985).
10. S.P. Antal, R.T. Lahey, J.E. Flaherty, "Analysis of Phase Distribution in Fully-Developed Laminar Bubbly 2-Phase Flow", *International Journal of Multiphase Flow*. **17**, pp. 635-652 (1991).
11. R.T. Lahey, D.A. Drew, "The Three-Dimensional Time and Volume Averaged Conservation Equations of Two-Phase Flow", in: Lewins J.B.M. (Ed.), *Advances in nuclear science and technology*, Plenum press, New York, NY, USA, pp. 1-69 (1988).
12. C.L. Vandervort, A.E. Bergles, M.K. Jensen, "The Ultimate Limits of Forced Convective Subcooled Boiling Heat Transfer", RPI Interim Report HTL-9 DE-FG02-89ER14019 (1992).
13. R.W. Bowring, A simple but accurate round tube uniform heat flux, dryout correlation over the pressure range 0.7-17MN/m^2 (100-2500 psia). *AEEW-R* 789(1972).